Journal of Biotechnology 205 (2015) 3–13

Contents lists available at ScienceDirect

Journal of Biotechnology

journal homepage: www.elsevier.com/locate/jbiotec

In vitro co-culture model of medulloblastoma and human neural stem cells for drug delivery assessment

Delyan P. Ivanov[a,*], Terry L. Parker[b], David A. Walker[c], Cameron Alexander[a], Marianne B. Ashford[d], Paul R. Gellert[d], Martin C. Garnett[a]

[a] School of Pharmacy, University of Nottingham, Nottingham, UK
[b] Medical School, Queens Medical Centre, University of Nottingham, Nottingham, UK
[c] Children's Brain Tumour Research Centre, Queens Medical Centre, University of Nottingham, Nottingham, UK
[d] AstraZeneca, Silk Road, Macclesfield, UK

ARTICLE INFO

Article history:
Received 19 August 2014
Received in revised form
22 December 2014
Accepted 5 January 2015
Available online 12 January 2015

Keywords:
Three-dimensional tumor model
Cancer drug screening in 3D
Co-culture spheroid
Human stem cell neurosphere
Medulloblastoma

ABSTRACT

Physiologically relevant *in vitro* models can serve as biological analytical platforms for testing novel treatments and drug delivery systems. We describe the first steps in the development of a 3D human brain tumour co-culture model that includes the interplay between normal and tumour tissue along with nutrient gradients, cell-cell and cell-matrix interactions. The human medulloblastoma cell line UW228-3 and human foetal brain tissue were marked with two supravital fluorescent dyes (CDCFDASE, Celltrace Violet) and cultured together in ultra-low attachment 96-well plates to form reproducible single co-culture spheroids (d = 600 μm, CV% = 10%). Spheroids were treated with model cytotoxic drug etoposide (0.3–100 μM) and the viability of normal and tumour tissue quantified separately using flow cytometry and multiphoton microscopy. Etoposide levels of 10 μM were found to maximise toxicity to tumours (6.5% viability) while stem cells maintained a surviving fraction of 40%. The flexible cell marking procedure and high-throughput compatible protocol make this platform highly transferable to other cell types, primary tissues and personalised screening programs. The model's key anticipated use is for screening and assessment of drug delivery strategies to target brain tumours, and is ready for further developments, e.g. differentiation of stem cells to a range of cell types and more extensive biological validation.

1. Introduction

Advancements in the treatment of cancer depend on physiologically relevant *in vitro* models to detect and prioritise novel drugs and drug delivery strategies. The use of reductionist monolayer cultures with non-physiological levels of oxygen (Carrera et al., 2010), combined with lack of cell–cell and cell–matrix interactions (Cukierman et al., 2001), often produce answers that are not representative of *in vivo* response. The likelihood of approval of emerging cancer therapies is currently below 10% (Hay et al., 2014), which is in part due to lack of reliable *in vitro* models (Astashkina et al., 2012).

Brain tumours are especially difficult to treat because of the challenges posed by the blood-brain barrier (Muldoon et al., 2007). The BBB limits the transport of many chemotherapy drugs and especially those which are hydrophilic, highly protein-bound or with molecular weight over 400 Da (Shen et al., 2004). Possible strategies to overcome the BBB are barrier disruption, blocking of efflux pumps, utilising transporters and local drug delivery (Deeken and Löscher, 2007). Local delivery to the brain can be achieved using convection enhanced systems (Barua et al., 2013), postsurgical delivery systems like Gliadel (Attenello et al., 2008), mouldable matrices (Rahman et al., 2013), or by infusion of drugs into the cerebrospinal fluid (Conroy et al., 2010).

In vitro modelling of local drug delivery to brain tumours can add in the rational design of drug delivery systems. Employing cultures of both normal and tumour tissue provides information for the relative safety and efficacy of treatment and can be used to rank formulations according to their therapeutic safety ratio (Hickman, 2014). Our previous studies (Meng et al., 2007) have indicated that using the correct dimensionality plays a significant role in modelling the physiological response of *in vitro*

* Corresponding author. Tel.: +44 0 115 84 68559.
E-mail addresses: paxdi@nottingham.ac.uk (D.P. Ivanov), terry.parker@nottingham.ac.uk (T.L. Parker), david.walker@nottingham.ac.uk (D.A. Walker), cameron.alexander@nottingham.ac.uk (C. Alexander), Marianne.Ashford@astrazeneca.com (M.B. Ashford), Paul.Gellert@astrazeneca.com (P.R. Gellert), m.garnett@nottingham.ac.uk (M.C. Garnett).

http://dx.doi.org/10.1016/j.jbiotec.2015.01.002

cultures. Fluorescently-labelled biodegradable nanoparticles were taken up six times more in tumour spheroids made of DAOY medulloblastoma cells compared to normal tissue (rat brain slices) when cultured together in 3D (Meng, 2006). These effects were only observed in three-dimensional cultures where the biologically appropriate cell interactions and physiological gradients were present. In order to increase the biorelevance of this model to humans and eliminate the pitfalls of interspecies differences (Rangarajan et al., 2004) we decided to pursue an improved version of the *in vitro* system employing only human tissues, cultured in scaffold-free spheroid cultures.

In our most recent *in vitro* model (Ivanov et al., 2014), medulloblastoma and stem cell spheroids were cultured in separate wells and analysed with a battery of multiplexable assays. However culturing both cell types separately did not allow for any interaction between the tumour cells and the normal tissue. The direct and paracrine tumour–host interaction has been repeatedly demonstrated to affect chemo (Straussman et al., 2012) and radiosensitivity (Upreti et al., 2011), proliferation (Spink et al., 2006), angiogenesis (Wartenberg, 2001), cell adhesion (Chambers et al., 2011) and gene expression (L Berg et al., 2014). Spheroid co-cultures have been used to demonstrate differential response to local intravesical treatment in bladder cancer (Kilani et al., 2003, 2002). Moreover, including a normal tissue component was proven to be vital in the successful development of lung cancer models (Amann et al., 2014). Therefore we have chosen to include the normal brain tissue in a co-culture with the tumours to provide a surrogate for tumour-host interactions and serve as an internal control for treatment toxicity.

There are a number of methods that can be used to distinguish between different populations of cells cultured together in co-cultures. Specific antigens can be employed (Kilani et al., 2003; Phan-Lai et al., 2013), cells can be genetically modified to express fluorescent proteins (Fang et al., 2013; Hsiao et al., 2009) and fluorescent dyes can be utilised for medium-term cell monitoring (Go et al., 1997).

Medulloblastoma is an embryonal tumour that shares many antigens with developing neural progenitor cells (Carpenter et al., 1999; Nagato et al., 2005; Srivastava and Nalbantoglu, 2008; Vanner et al., 2014; Zanini et al., 2013). The common antigen presentation precludes the use of specific antibodies to distinguish between developing brain tissue and the tumour cells. Moreover, medulloblastoma is made up of least four clinically and molecularly distinct types of tumours (Taylor et al., 2012). There appear to be further differences within subgroups (Kool et al., 2014; Shih et al., 2014) as well as intratumoral heterogeneity especially after treatment with radiation and chemotherapy (Ramaswamy et al., 2013). In this respect using genetic manipulation to mark the cells would lead to single clone selection and limit the usefulness of the system by eliminating heterogeneity. Therefore, marking with fluorescent supravital dyes was chosen as the best method for cell tracking because of its flexibility, no requirement for specific antigens, and compatibility with primary tissue due to tissue heterogeneity preservation.

We have employed a suite of imaging and analytical techniques to characterise the co-cultures and quantify the number and health status of the labelled cells. Microscopy-based analysis offers the opportunity to image the intact spheroids and reveal the spatial distribution and interaction between both cell types. However, confocal microscopy is limited by the penetration depth of short wavelength photons and can cause considerable tissue photobleaching. In contrast, multiphoton microscopy uses longer wavelength photons which can penetrate deeper into the spheroids. Both microscopy techniques are limited in the number of fluorophores they can analyse and spectral overlap can be a significant problem.

Flow cytometry circumvents the abovementioned obstacles by illuminating the cells with light from different lasers and detecting the emitted fluorescence in a number of separate channels. While flow cytometry does not reveal the 3-D organisation within the co-culture, it has a larger dynamic range than fluorescence microscopy and is less susceptible to fluorescence interference. It also allows the use of more colours and provides superior data handling tools compared to the analysis of multiphoton images. Hence it was the preferred mode for stem cell and tumour population quantification and determination of cellular health status.

Here we report a proof of concept study in the technical development of a co-culture *in vitro* model of human medulloblastoma to use as an assessment tool for drug delivery. The model utilises the UW228-3 cell line and human foetal brain tissue cultured as neurospheres in defined serum-free stem cell media. The medulloblastoma cell line was chosen to mimic small foci of left-over tumour tissue after surgery and leptomeningeal metastases. These cells were cultured together with foetal human brain tissue enriched for progenitor cells to represent, in model form, a developing child's brain. Etoposide was used as a clinically-important cytotoxic drug to test the safety and efficacy of local chemotherapy aimed at brain tumours.

2. Materials and methods

2.1. Materials

Dulbecco's Phosphate Buffered Saline (PBS), Dulbecco's Modified Eagle's Medium - high glucose (DMEM), Ham's nutrient mixture F12, L-Glutamine, Heparin, Sodium pyruvate and etoposide were obtained from Sigma–Aldrich (Dorset, UK).

Foetal Bovine Serum (FBS), N2 supplement, B27 serum-free supplement, DMEM without phenol red, basic human Fibroblast Growth Factor (bFGF), human recombinant Epidermal Growth Factor (EGF), Accutase, CellTrace Violet and 5-(and-6)-carboxy-2′,7′-dichlorofluorescein diacetate succinimidyl ester (CDCFDASE) were supplied by Invitrogen (Paisley, UK).

Annexin V-Allophycocyanin (Annexin-APC, 20X solution) and 7-Aminoactinomycin D (7-AAD, 50 μg/ml) were purchased from Ebioscience (Hatfield, UK).

Ultra low attachment (ULA) 96-well round bottom plates were obtained from Corning (Amsterdam, The Netherlands)

2.2. Cell lines and culture

All experiments were performed in standard cell culture conditions at 37 °C and 5% CO_2.

UW228-3 medulloblastoma cell line (Keles et al., 1995) was obtained from Prof. Silber (University of Washington, Seattle, USA) with the help of the Children's Brain Tumour Research Centre at the University of Nottingham. UW cells were cultured in DMEM/F12 media supplemented with L-Glutamine (2 mM), sodium pyruvate (1 mM) and FCS (10%). Subculturing was performed using 0.025% Trypsin in Ca^{2+} and Mg^{2+} free PBS solution for 5 minutes.

Foetal human brain tissue was received from the Joint MRC/Wellcome Trust (grant # 099175/Z/12/Z, Ethics committee approval 08/H0906/21 + 5, Health Research authority NRES Committee North East - Newcastle & North Tyneside 1) Human Developmental Biology Resource (www.hdbr.org). The tissue was rinsed, mechanically dissociated into a single cell suspension and cultured in non-treated flasks to form stem cell enriched neurospheres (Uchida et al., 2000).

The Neural stem cell (NSC) defined serum-free media was made using DMEM/F12 (1:1), B27 (1:50), N2 (1:100), L-Glutamine (2 mM), hEGF (20 ng/ml), bFGF (10 ng/ml) and Heparin (5 μg/ml).

Neurospheres were subcultured for less than 15 passages. Briefly, when the neurospheres reached a diameter of 100–300 μm they were rinsed with PBS, resuspended in Accutase (1 ml) and agitated for 5 min at 37 °C followed by mechanical dissociation. The suspension was diluted with fresh NSC media and centrifuged at 300 g for 5 min. The cell pellet was resuspended in Ca^{2+} and Mg^{2+} free PBS and the final single-cell suspension diluted to the desired concentration with NSC media.

2.3. Cell label optimisation experiments

Cell marking optimisation screening was performed with UW and NSC cells with both CellTrace Violet and CDCFDASE in concentrations ranging from 2.5 to 20 μM.

UW228-3 (UW) cells were labelled in monolayers prior to culturing as spheroids. Cells, grown to 80% confluence in cell culture treated flasks, were washed twice with HBSS (with Ca^{2+} and Mg^{2+}) and incubated with 2.5–20 μM concentrations of CDCFDASE and CellTrace Violet in HBSS (with Ca^{2+} and Mg^{2+}) for 30 min at 37 °C. Afterwards they were washed twice with HBSS and incubated for further 3–4 h in FCM in order to remove any unconjugated dye. The labelled cells were dissociated using 0.025% Trypsin

Neural stem cell (NSC) spheroids were dissociated and the cell suspension was incubated with 2.5–20 μM concentrations of CDCFDASE and CellTrace in HBSS for 30 min at 37 °C.

Both cell types were seeded in ultra-low attachment plates (200 μl, 7000 cells per well). The plates were centrifuged lightly at 100 g for 3 min after seeding and the cells organised into one single spheroid per well within 24 h. Controls of unstained cells of each type were included in every plate. Old media were carefully exchanged with fresh media (150 μl) on days 3 and 5. Spheroids were cultured for 7 days before final analysis.

The effect of both cell marker dyes on spheroid proliferation and metabolic activity were assessed by comparing marked spheroid volume and metabolic activity to unstained controls. Flow cytometry was used to assess dye retention in each condition.

2.4. Co-culture formation

Co-culture spheroids were established by plating a homogenous mix of fluorescently labelled tumour and stem cells (200 μl, 3500 cells/well from each type) as a single-cell suspension in ULA plates at the same time. Co-culture spheroids formed in 24 h and were cultured for 7 days, exchanging with fresh media (150 μl) on days 3 and 5.

2.5. Spheroid viability monitoring

Spheroid growth was monitored using an Olympus CKX41 microscope with a 10X objective and an attached Olympus E330 camera. The scale of images was determined using a calibration slide. Images were analysed using a specially written macro (Ivanov et al., 2014) for the open-source software ImageJ (Fiji 2013 package) and spheroid area was used to calculate the volume of an equivalent sphere as a proxy for growth and viability.

Spheroid metabolic activity was determined using Resazurin reduction. On day 7 the old media in each well were exchanged for fresh media (150 μl) supplemented with Resazurin (60 μM) from a freshly-thawed stock solution (440 μM). Spheroids were placed for 4 h in the incubator and fluorescence was measured with an excitation wavelength of 530 nm and emission 590 nm on a Galaxy Fluostar plate reader.

2.6. Multiphoton confocal microscopy

Spheroids were fixed using polyformaldehyde solution (4%) after washing twice with PBS (150 μl). The spheroids were stored in the plates at 4 °C in PBS protected from light. Imaging was done by placing the spheroids on top of a glass slide along with 20 μl of PBS. Zeiss LSM510NLO confocal multiphoton microscope was used with a Plan-apochromat 20x/0.8 objective and 800 nm excitation wavelength. Images were later processed using ImageJ by auto-adjustment of brightness and contrast, followed by creating an average intensity Z-projection.

Table 1
Dye combination and detection configuration used in the Flowsight imaging flow cytometer.

Dye	Function	Excitation	Emission
CellTrace Violet	Cell label (UW228-3)	405	Channel 7 (430–505)
CDCFDASE	Cell label (NSC)	488	Channel 2 (505–560)
7-AAD	Dead and apoptotic cells	488	Channel 5 (642–740)
Annexin-V	Early apoptotic cells	642	Channel 11 (642–740)

2.7. Cytotoxicity screen

Labelled spheroid co-cultures were seeded in ULA plates and exposed to increasing concentrations (0.3–100 μM) etoposide on day 3. Etoposide was replaced with fresh media on day 5 and analysed on day 7. Controls included in the screen were unstained single cultures of UW and NSC cells, unstained co-culture, single colour controls and labelled co-culture control with media and DMSO (0.2%). Six spheroids per condition were analysed on each plate. Brightfield images of the cultures were used to determine the volume of the spheroids compared to untreated controls. The percentage of each population was estimated using flow cytometry.

2.8. Flow-cytometry

Spheroids were washed twice with PBS (150 μl/well), dissociated using Accutase (double concentrated, 50 μl/well) for 30 min at 37 °C followed by mechanical dissociation by repeated pipetting. The resultant single cell suspensions from six wells per condition were pooled together in a microcentrifuge tube, centrifuged (300 g, 5 min) and resuspended in Annexin binding buffer (10 mM HEPES, 140 mM NaCl, 2.5 mM $CaCl_2$ pH = 7.4; 50 μl). Dead and apoptotic cells were stained using 7-AAD (5 μl, 50 μg/ml) as per (Zembruski et al., 2012). Early apoptotic cells were detected using Annexin V-APC (2.5 μl). After incubation for 15 min in the dark, further Annexin binding buffer (200 μl) was added and the cells stored on ice, protected from light were analysed within 2 h. Flow cytometry experiments were done using a 14 channel MoFlo XDP cell sorter (Beckman Coulter) equipped with a three laser system (405, 488 and 630 nm). CDCFDASE and 7-AAD positive cells were detected using the blue 488 nm laser and the 529/28 and 670/30 channels respectively. CellTrace Violet positive cells were excited with the violet 405 nm laser and detected with a 450/65 filter. The Annexin V-APC positive apoptotic cells were excited by the red 630 nm laser and detected in the 670/30 channel. Non-stained and single colour controls were included in each experiment. Data were analysed using the Weasel software package. Debris were identified and subsequently excluded by gating the Annexin V-APC and 7-AAD negative population on the Forward/side scatter dot plot and selecting for the particles with the lowest forward scatter values (Duggan, 2012).

2.9. Imaging flow cytometry

Imaging flow cytometry using the Amnis Flowsight system was used to visualise the dissociated cells from the spheroid co-cultures. The following combination of lasers and detectors was employed (Table 1). Non-stained and single colour controls

were used to calibrate the channels and data were analysed on the AMNIS IDEAS Software.

2.10. Data analysis and statistical analysis

Raw data from volume determination, Resazurin reduction, and flow cytometry software were exported and analysed in MS Excel and Graphpad Prism 6. In label optimisation experiments, readings were normalised to the relevant unstained control (100%) and spheroid-free wells (0%). In cytotoxicity experiments, volume measurements were normalized so that untreated co-culture controls were assigned to 100% viability and media-only wells- 0% viability. Flow cytometry results for the proportion of stem cells and tumours were multiplied by the volume of each spheroid to estimate the surviving fraction of each cell type. Dose response curves were fitted using the four-parameter logistic equation in Prism, the top was constrained to 100% and the bottom to 5%. Results are displayed as mean ± SD unless stated otherwise. There were $n = 6$ replicates for each condition in each individual experiment and displayed data represent the mean of at least three independent experiments.

3. Results

3.1. Cell marking optimisation

The first task in establishing the co-culture models was to make sure that both cell types (UW and NSC cells) could be reliably distinguished from each other. A dye optimisation experiment was performed in order to investigate which marking strategy would be most suitable for marking for each of the two cell populations. It aimed to establish the most favourable concentration to label the cells specifically without pronounced toxic effects. UW228-3 and NSC cells were marked with CDCFDASE and CellTrace Violet in concentrations ranging from 2.5 to 20 μM. Fig. 1 shows the impact of dye concentration on the frequency distribution of cellular fluorescence in the fluorescent channels of CDCFDASE and CellTrace Violet. Despite the low mean fluorescence of non-marked UW cells, dye concentrations lower than 10 μM did not shift the population's fluorescence distribution at day 7 far enough to achieve a good separation from the control. As seen in Fig. 1A and B the optimal staining concentration for the tumours was 10 μM for both dyes and little was gained from increasing dye levels to 20 μM. The stem cell population on the other hand showed a very pronounced difference in the distribution of the fluorescence signal with increasing dye concentrations. Fig. 1C illustrates the gradual shift of the fluorescence for the whole stem cell population and clearly shows that CellTrace Violet can effectively mark the cells at levels as low as 5 μM. CDCFDASE followed a similar trend in Fig. 1D although the shift was less pronounced when compared to CellTrace Violet. Overall, in the conditions tested, CellTrace Violet was superior in marking the cells compared to CDCFDASE because it elicited a more pronounced shift in the fluorescence of both cell types.

Table 2
Marking UW-228 and NSC cells with supravital dyes CDCFDASE and CellTrace Violet. Percentage of positive cells is given compared to unstained control.

Condition	% Positive cells	
	UW228-3	NSC
Control	2	2
CellTrace 2.5 μM	63	74
CellTrace 5 μM	71	94
CellTrace 10 μM	90	99
CellTrace 20 μM	96	100
CDCFDASE 2.5 μM	–	50
CDCFDASE 5 μM	77	93
CDCFDASE 10 μM	86	98
CDCFDASE 20 μM	85	99

These results were confirmed when the relative percentages of cells with fluorescence brighter than control were compared in Table 2. The data demonstrates that levels of 10 μM were needed to stain tumour cells and 5 μM were sufficient for stem cells for both dyes. Although these data indicated a combination of 10 μM CellTrace Violet for the UW and 5 μM CDCFDASE for the NSC might be advantageous, the superiority of this combination became visually apparent after comparing the dot plots in Fig. 2.

Fig. 2 shows the rationale behind choosing the appropriate dye for the stem cells and tumours. Complete and effective resolution of the two populations is only achieved by using CDCFDASE for

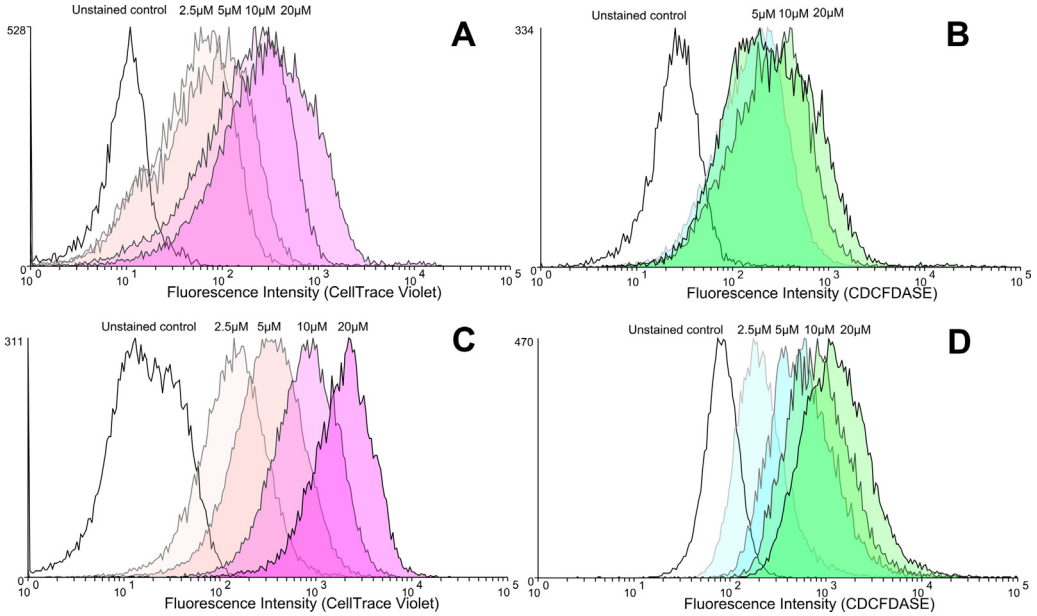

Fig. 1. Histograms of the frequency distributions of long-term fluorescent labelling for UW and NSC cells labelled with CellTrace Violet and CDCFDASE (Green). A- UW cells marked with CellTrace Violet, B-UW cells marked with CDCFDASE, C-NSC cells marked with CellTraceViolet, D-NSC marked with CDCFDASE.

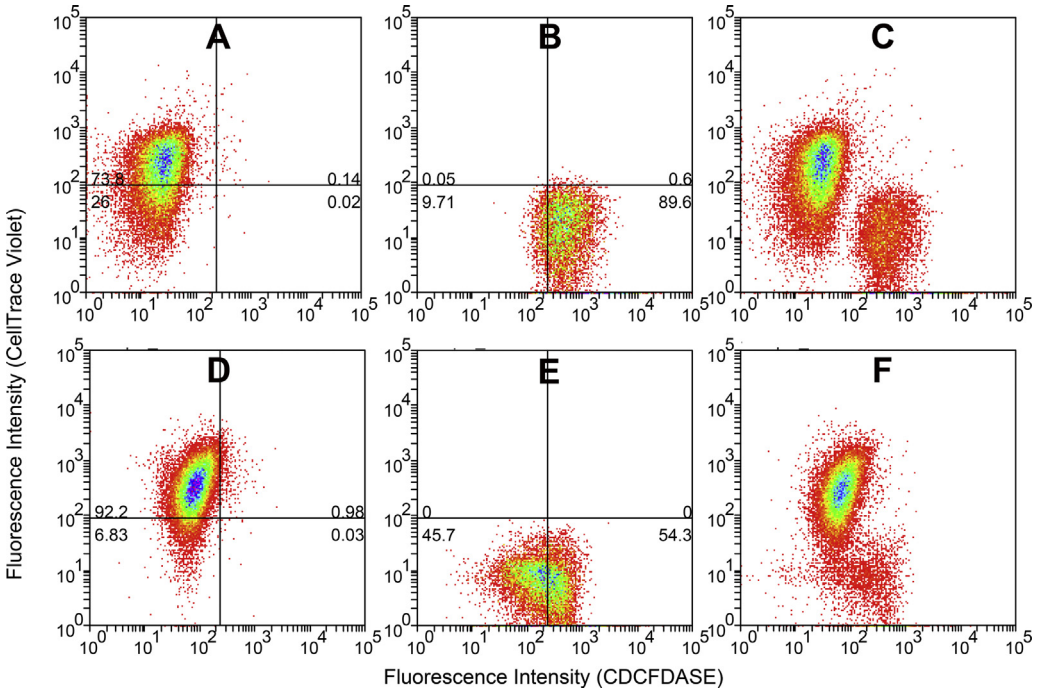

Fig. 2. Two dimensional dot plots showing single and mixed populations of UW and NSC cells marked with both dyes. X-axis shows intensity of fluorescence in the CDCFDASE channel, Y-axis fluorescence intensity in the CellTrace Violet channel. Quadrants are defined by the autofluorescence intensity values for the unstained stem cell population which are within the lower left quadrant of the plots A- UW marked with 10 μM CellTrace Violet, B- NSC marked with 5 μM CDCFDASE, C- mix of UW-CellTrace Violet and NSC-CDCFDASE, D-NSC marked with 5 μM CellTrace Violet, E- UW marked with 10 μM CDCFDASE, F- mix of UW-CDCFDASE and NSC-CellTrace Violet.

the foetal tissue and CellTrace Violet for the tumours (Fig. 2C). This cell discrimination can be explained with the higher autofluorescence of stem cells compared to tumours. CellTrace Violet achieves a more pronounced shift in fluorescence for the tumours which, combined with their intrinsically low autofluorescence in the CDCFDASE channel, leads to better separation from the stem cell population. In contrast the small shift in UW cell fluorescence achieved by CDCFDASE is sufficient to distinguish them from unstained tumour cells but not enough to differentiate them from the stem cells (Fig. 2F).

In order to investigate the effect of marking the cells with fluorescent dyes on spheroid viability and growth, the volume and metabolic activity of stained spheroids were compared to unstained spheroids of UW and NSC cells. Fig. 3A shows that stem cells treated with increasing concentrations of each dye yielded smaller spheroids after 7 days of culture compared to untreated controls. This effect was less pronounced for UW spheroids which were only affected at concentrations above 10 μM. Nevertheless, metabolic activity (Fig. 3B) for all spheroids, as determined by Resazurin reduction, was above 80% when dye concentration was kept below 10 μM. Fig. 3C shows the volume of marked spheroids made of UW of NSC cells marked with 10 μM CellTrace Violet and 5 μM CDCFDASE respectively. The results of five independent experiments showed that while stem cells produced 30% smaller spheroids than unstained controls, tumours were less affected by the dying procedure and only had 10% lower volume compared to controls.

3.2. *Effects of etoposide treatment*

After the initial optimisation experiments the marked tumour and stem cells were seeded and cultured together in co-culture mimicking the interaction between normal brain and tumour tissue (Fig. 4). These co-cultures were allowed to grow for 3 days before they were exposed to etoposide for 48 h followed by another 2 days in etoposide-free media. The right panel in Fig. 4 shows light microscopy images of the spheroids after 7 days of culture along with the conditions in each column.

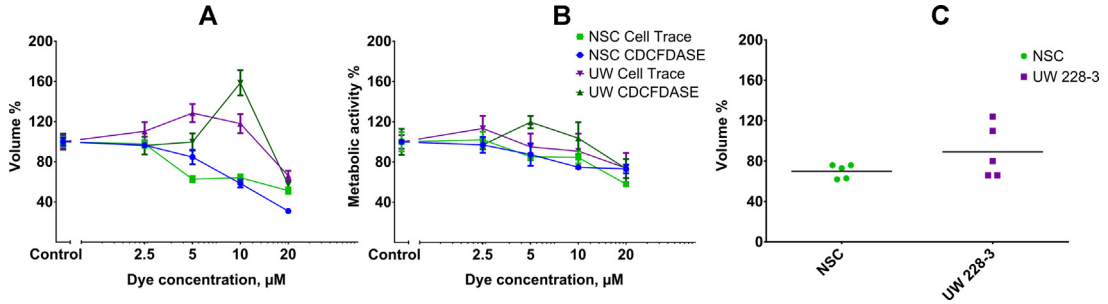

Fig. 3. Volume and metabolic activity of spheroids marked with the supravital dyes compared to unstained controls A-Volume of UW and NSC spheroids marked with different levels of fluorescent dyes after 7 days of culture compared to unstained controls. B- Metabolic activity of the same spheroids measured as resazurin reduction compared to control. C- Volume of stem cell and tumour spheroids stained with 5 μM CDCFDASE and 10 μM CellTrace Violet respectively compared to unmarked controls.

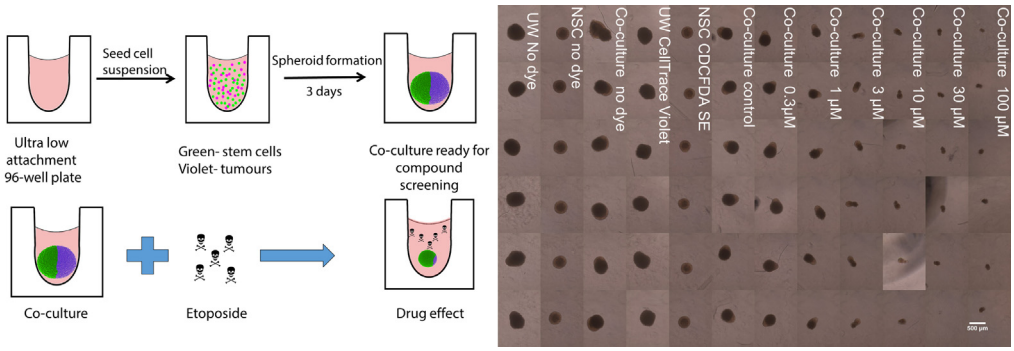

Fig. 4. Medulloblastoma *in vitro* model experimental setup. Left panel- co-culture formation in overlay and etoposide exposure. Right panel- 96-well plate experiment phase contrast microscopy image after 7 days of culture along with conditions for each column. Scale bar is 500 μm.

Fig. 5 shows the light and multiphoton microscope images of the co-cultures and the flowchart for flow cytometry gating and analysis. The multiphoton images reveal the spatial distribution of the two cell populations while flow cytometry was used to quantify the proportion of each cell type. Despite seeding the cells together in the form of a mixed single cell suspension, the cells organised themselves into polarised spheroids with discrete tumour-dominated and stem cell-dominated regions. As seen in the images, there were tumour cells detectable within the stem cell part, resembling metastases, and a fraction of double positive cells whose origin could not be identified solely on the basis of imaging. Flow cytometry after spheroid dissociation was used to quantitate the ratio of tumour and stem cells within the mixed cultures and monitor the effects of etoposide. The stem cells were well segregated from the tumours due to the bright CDCFDASE staining. The double-positive cells, which were highly fluorescent in both channels, were clearly separated from the tumour population and clustered with the stem cells. Each population was further examined for apoptosis-related phosphatidylserine externalisation using Annexin V-APC (Koopman et al., 1994) and for 7-AAD uptake (Zembruski et al., 2012) to infer cell death.

Etoposide addition profoundly altered the ratio of tumours to stem cells in the spheroids. As seen in Fig. 6, with increasing etoposide concentration the tumour cell proportion dropped significantly and reached its lowest point at 10 μM etoposide. Although both populations started at similar numbers, increasing etoposide concentrations primarily targeted the tumours and at 10 μM the spheroids were composed predominantly of stem cells. This is in agreement with the results from the two photon confocal microscopy shown in the bottom panel. The average intensity z-stacks show a progressive elimination of the tumour cells with only traces of these cells left at the 10 μM concentration. Nevertheless, the decrease in tumour burden was not wholly advantageous and higher etoposide concentrations elicited a shrinkage of the spheroid as a whole, indicating toxicity to the stem cells as well.

Dose-response curves were extrapolated by using the volume of the co-culture spheroids and the proportion of stem-cells to tumour cells determined by flow cytometry in order to fully describe the effects of etoposide on both populations. The resultant values were normalised to the initial values for stem cells and tumours respectively and the results plotted in Fig. 7A. Despite the variability between the different experiments there was a clear dose-response trend in which stem cell viability was lower or equal to that of tumours below 3 μM and higher at etoposide levels between 3 and 10 μM. The most favourable etoposide concentration 10 μM when the viability of NSC (41%) was 6 times higher than tumour viability

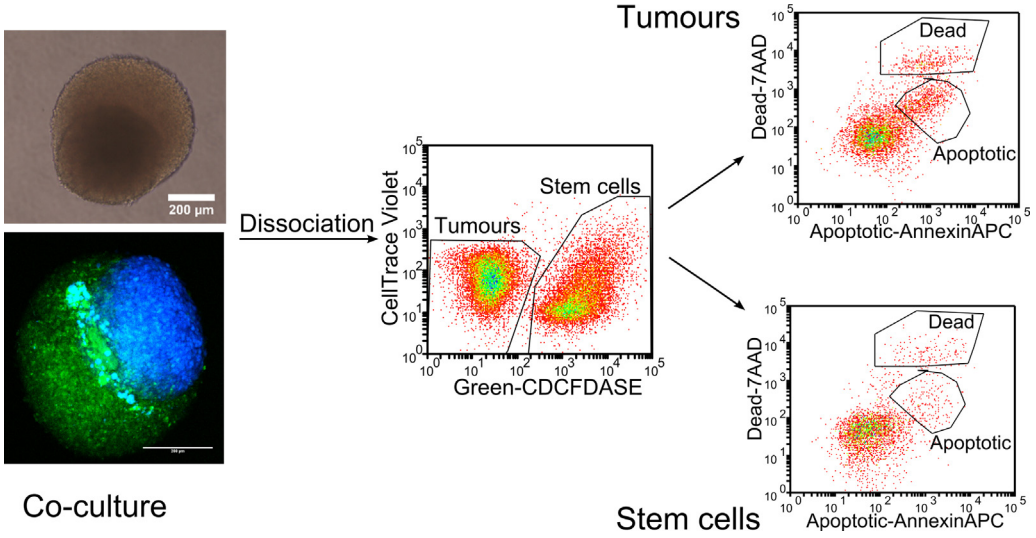

Fig. 5. Medulloblastoma co-culture model analysis. Top left- phase contrast microscopy image of co-culture spheroid. Darker sphere is made up of UW cells while brighter cells are NSC. Bottom left multiphoton average intensity z-stack projection image of co-culture spheroids. Green cells represent NSC, blue cells–UW228-3 and Cyan-double positive cells. Scale bars 200 μm. After dissociation into single cells spheroids were analysed using flow cytometry. Middle dot plot panel shows that tumour and stem cell populations can be gated separately owing to their different fluorescence in both channels. Double positive cells in middle dot plot appear to cluster with stem cells. Right dot plots show tumour (top panel) and stem cells (bottom panel) assayed separately for viability using Annexin-APC for apoptotic cells and 7-AAD to mark dead cells. Note that living cells have low 7-AAD fluorescence, apoptotic medium and dead-high as described by Zembruski et al., 2012.

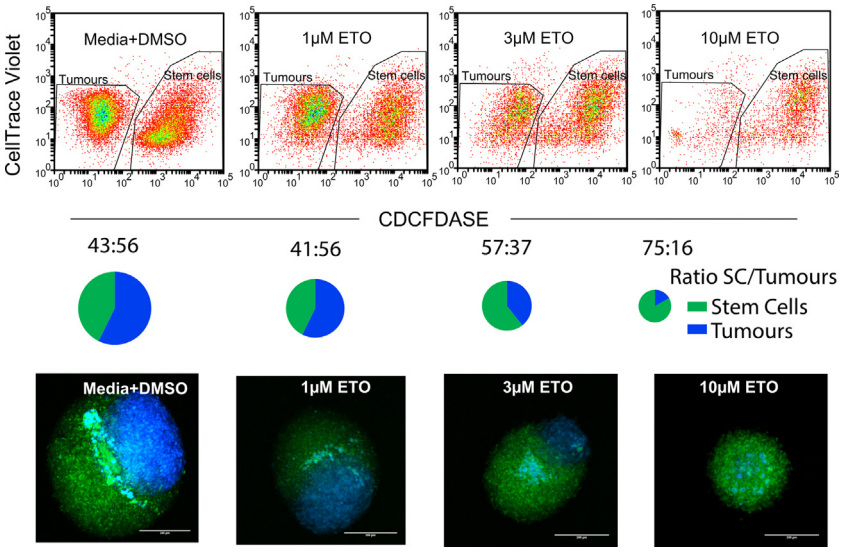

Fig. 6. Co-cultures exposed to different levels of etoposide. Dot plots and multiphoton images. The top panel shows dot plots for the live cells in the spheroid. Top left plot represents the living cells in the controls, cultured in media and DMSO. The dot plots are marked with the relevant etoposide concentration in μM. The proportional increase of stem cell to tumours shown in the dot plots is represented by the pie charts of the middle row. Increasing concentrations of etoposide gradually eliminated the tumours cells. Bottom row shows multiphoton microscope average intensity z-stacks of spheroids cultured at the above conditions. Blue cells are UW tumours, green cells are stem cells and scale bars are 200 μm.

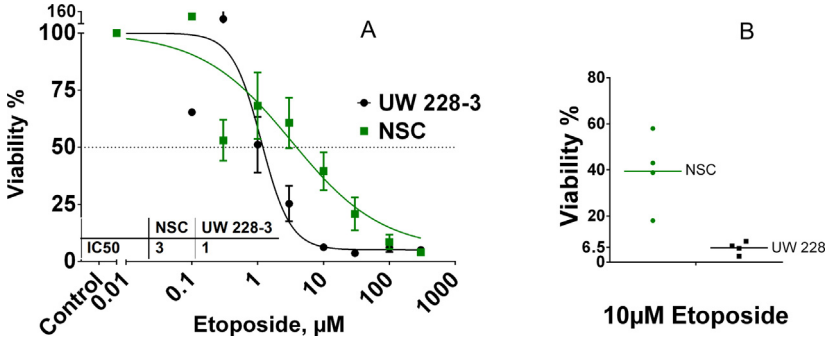

Fig. 7. Dose-response data for co-cultures of neural stem cells and UW medulloblastoma cells exposed to etoposide. A-Comparison of viability for each population calculated from the total volume of the co-culture spheroid (image analysis) and the ratio between stem cells and tumours (flow cytometry). Error bars represent SEM for $n = 4$ independent experiments B- comparison of the viability of stem cells and tumours at 10 μM etoposide, dots represent separate experiments. Note the high inter-experimental variability of the data for the stem cells and the narrow distribution for tumours. IC50 for stem cells was calculated to be 3 μM (95%CI = 2–7 μM) and 1 μM (95% CI = 0.8–2 μM) for UW228-3 cells.

(6.5%) as shown in Fig. 7B. This was a statistically significant difference as determined by a two-tailed t-test with Welch's correction for unequal variance ($p = 0.0257$). The observed higher viability of stem cells at 10 μM etoposide is in agreement with the results from our previous study in separate cultures of unlabelled stem cell and tumour spheroids (Ivanov et al., 2014).

In addition to the conventional flow cytometry experiments, imaging flow cytometry was employed in order to visualise and better characterise the separate populations (Fig. 8). The stem cells gave a bright signal in the green channel whereas the tumours were positive for CellTrace Violet fluorescence. The membrane distribution of phosphatidylserine in apoptotic cells was also visualised. In addition the double positive cells were confirmed to be stem cells that had small particles attached to them responsible for the high-fluorescence in the violet channel.

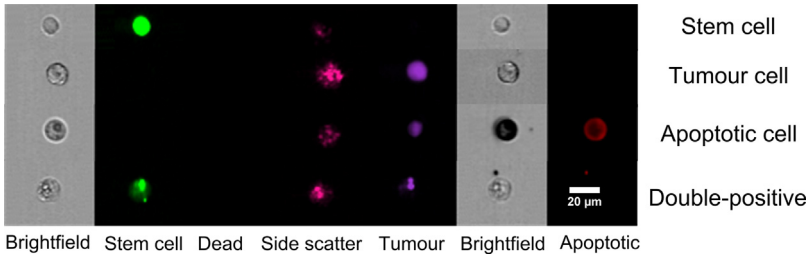

Fig. 8. Imaging flow cytometry- representative examples of the different cell populations. Stem cells are positive in the green channel, while tumours are registered in the violet channel. Apoptotic cells show a membrane associated fluorescence in the AnnexinV-APC channel with in agreement with externalisation of phosphatidylserine. Blebs on double-positive cells register on both the green and the violet channels.

4. Discussion

The most common strategies for long-term supravital fluorescent cell marking involve either marking the cell membrane with lipophilic carbocyanine dyes (Honig and Hume, 1986), or preferential cytosolic protein marking with amine-reactive compounds (Weston and Parish, 1990). Nuclear staining dyes like Hoechst 33342 were not considered because of their reported DNA interaction and short-lived labelling (Samlowski et al., 1991). The thiol-reactive CellTracker Violet (BMQC) appeared to be toxic to the cell lines tested (data not shown) and was excluded as well. Despite the proven track record of carbocyanine dyes in neuron labelling their fluorescence staining can often diminish before analysis (Chintala et al., 1997) and dye transfer to the nearby cells has been reported (Khoshyomn et al., 1998; Lassailly et al., 2010; Nygaard et al., 1998).

The amine-reactive dyes have been reported to be superior in peak resolution and non-specific dye transfer compared to the membrane-staining dyes (Begum et al., 2013) CDCFDASE is the 2,7-dichloro derivative of CFDA SE (Parish, 1999) which is less susceptible to photobleaching and pH fluctuations. Both CDCFDASE and CellTrace Violet share the same mechanism for marking the cells- acetate groups allow the molecules to cross the cell membrane and are subsequently cleaved in the cytoplasm. Afterwards the succinimidyl moiety reacts with amino groups of cytosolic proteins and labels the cells for about 5–8 cell divisions (Quah and Parish, 2012). This staining strategy can be used on any cell type and is substantially less toxic compared to chloro- and bromo-methyl reactive dyes that bind to cellular glutathione.

We were able to utilise both CDCFDASE and CellTrace Violet in our co-culture model and maintain a high level of cellular fluorescence for 7 days. CellTrace Violet yielded a bigger shift in fluorescence compared to CDCFDASE and did not affect the medulloblastoma spheroid volume or metabolic activity. Although the final stem cell neurosphere volume was 30% lower than the unstained controls, the decreased sphere volume did not translate to reduced metabolic activity up to levels of 10 μM of CDCFDASE and CellTrace Violet.

Spheroid co-cultures have been extensively used for invasion experiments in glioblastoma (Chintala et al., 1997; Go et al., 1997; Terzis et al., 1997a, 1997b; Thorsen et al., 1997). These studies have highlighted the importance of having a normal tissue component as well as the tumour cells. However these experiments relied on techniques like agar overlay which produced spheroids of varying, poorly reproducible sizes which necessitated manual sorting and decreased throughput. In most of these studies the tumour spheroids were exposed to the drug alone and only afterwards co-cultured with the normal tissue. In contrast to other reports, which have employed a single cell label (Amann et al., 2014), marking both cell populations increased the fidelity of cell type determination. Similarly, employing cytoplasmic dyes instead of membrane markers (Nygaard et al., 1998, 1995) resulted in stable marking for over 7 days with decreased dye loss or exchange between the two populations. Although other researchers have demonstrated the feasibility of differential cytotoxicity determination in co-culture spheroids (Kilani et al., 2003, 2002), their cell labelling strategy was only possible for cells with differential antigen expression and was not suited for heterogeneous cell populations. Therefore we have solved a number of practical challenges associated with the production of reproducible co-culture spheroids in a high-throughput compatible format and offer an improved labelling procedure well-suited for heterogeneous primary tissue.

A key technical problem with 3-D image analysis, is that confocal microscopy can only achieve 50–100 μm penetration in tissues (Indovina et al., 2007). We have attempted to tackle this problem by using two-photon microscopy. The multiphoton microscopy technique employed in this study allows the imaging of intact spheroids by using longer wavelength photons compared to conventional confocal microscopy. These lower-energy photons penetrate deeper into the spheroids and reveal the intrinsic 3D distribution of each cell type within the spheroid. Moreover multiphoton microscopy is more benign to tissue by limiting out-of-focus phototoxicity and photobleaching (König et al., 2011).

Strikingly, although the tumours and stem cells were seeded as a mix, they organised themselves into two poles- one enriched for tumour and one for normal tissue. Additionally, as seen in Figs. 5 and 6 there were a number of tumour foci within the normal tissue mimicking tumour invasion into the brain parenchyma. Spontaneous organisation of spheroids has been reported before (Urich et al., 2013) and is probably driven in this case by cell-cell recognition mechanisms. This is in agreement with the differential adhesion hypothesis postulated by Steinberg where spontaneous tissue segregation and sorting is thought to be guided by differential expression of cadherins, causing differences in surface tension between cell types (Foty and Steinberg, 2005). In previous work (Meng et al., 2007) we have seen invasion of DAOY medulloblastoma spheroids into organotypic cultures of rat neonatal cerebellum compared to cortical slices, which are not invaded significantly by DAOY spheroids suggesting that the cues for this cell behaviour can be very specific. Such interactions are reminiscent of the 'seeds and soils' hypothesis regarding the recognition between cancer and normal cells and the spread of metastasis to specific parts of the body (Langley and Fidler, 2011). The segregation behaviour exhibited in our model *in vitro* is in agreement with the growth and metastasis of tumour *in vivo*. Medulloblastoma presents initially as a single tumour mass in the posterior fossa separate from the cerebellum and when it metastasizes it colonises the craniospinal axis in small clumps (foci).

The combination of two dyes made it possible to assess the proportion of each cell population within the spheroid using flow cytometry after spheroid dissociation into single cells. The quantitative analysis of multiphoton images revealed the presence of double positive cells whose identity was investigated by conventional and imaging flow cytometry. The double positive cells visible in Figs. 5 and 6 clustered with the stem cell population in conventional flow cytometry dot plots. Moreover the image-based flow cytometer visualised those cells as stem cells with uniform green fluorescence and small particles with bright violet/blue fluorescence attached to the outside of the cells (Fig. 8). With increasing etoposide concentration the main tumour mass was almost completely eliminated but some small groups of tumour cells remained within the core of the spheroid.

The 3D co-culture model described here is made by simply mixing the NSC and UW cells in a high-throughput compatible 96-well format. No manual sorting, spheroid transfers or mixing are required and all steps could potentially be automated to increase productivity. The 96-well format allows the screening of a large number of formulations and the elucidation of dose-response relationships. Furthermore we have included human foetal brain tissue to understand better the off-target effects of local chemotherapy on the developing brain and put the inhibitory drug concentrations into clinical perspective. By harnessing these advantages we were able to pinpoint a therapeutic range for etoposide between 3 and 10 μM which maximises toxicity to tumours while stem cell viability remains 6 times higher. These values are in agreement with studies showing etoposide toxicity in the micromolar range in medulloblastoma (Nör et al., 2013; Othman et al., 2014; Tomlinson et al., 1991; Von Bueren et al., 2011) and a tenfold increase in resistance for spheroids (Luo et al., 1998). This concentration of etoposide can be achieved in patients by employing local intrathecal therapy (Fleischhack et al., 2001; Slavc et al., 2003). Using IC50 values for tumour cell lines in isolation is of little value because

they do not translate directly to *in vivo* response. Relative toxicity to normal and tumour tissue in the same compartment of the body can better inform on potential side effects and therapeutic windows. Therefore the inclusion of normal tissue not only increases the biological relevance of the model by including tumour–host interactions but also gives a unique strength in that the normal cell population serves as an internal control and "calibrates" the IC50 values of the assay.

The toxicity to neural progenitors shown by the model has also been reported in mice (Nam et al., 2010). These findings are in agreement with studies that have demonstrated the damaging potential of cytotoxic drugs to progenitor cells in the subventricular zone (SVZ), dentate gyrus (DG) and the corpus callosum (Dietrich et al., 2006). It should be noted, however, that the neurodevelopmental toxicity effects demonstrated by this *in vitro* model would only be replicated in patients if etoposide were to diffuse into the SVZ and DG at high enough levels. Leptomeningeal tumour metastases are in direct contact with the CSF and will receive the highest exposure to etoposide. In contrast progenitor cells in the SVZ are located tens of micrometres away from the wall of the lateral ventricle behind a layer of ependymal cells and a hypocellular layer (Barbaro et al., 2004; Quiñones-Hinojosa and Chaichana, 2007). Neurotoxic side effects in patients have been reported for other cytotoxics like cisplatin (Gregg et al., 1992), methotrexate (Bhojwani et al., 2014; Shuper et al., 2000) and cytarabine (Gállego Pérez-Larraya et al., 2011) but not for intrathecal etoposide (Fleischhack et al., 2001; Slavc et al., 2003; Van der Gaast et al., 1992) yet. Nevertheless, the findings in this study show that etoposide can damage proliferating cells regardless of their origin and suggest that more targeted approaches like nanoparticle encapsulation (Meng et al., 2007) should be considered to improve selectivity. Drug delivery strategies that limit normal tissue exposure and maximise the toxic effects to tumours are needed in order to prevent off-target toxicity.

The UW228-3 cell line used in this study is reported to be similar to either Sonic hedgehog driven (SHH) (Pambid et al., 2014) or Group 3 (Othman et al., 2014) medulloblastoma. Local interstitial therapy at the tumour bed may be most advantageous in SHH medulloblastoma as it tends to recur mainly locally (Ramaswamy et al., 2013). In contrast to that, the dismal prognosis and the frequent leptomeningeal metastases associated with Group 3 may favour the use of local intra-CSF delivery. Nevertheless, the chosen cell line was used as a model serving to establish the methodology of the assay and subsequent studies would include primary tumour tissue from patients.

The results from this study are supported by our previous work where the stem cells and the UW228-3 cell line were cultured separately without previous labelling (Ivanov et al., 2014). Despite the slight differences in the calculated IC50s and the loss of resolution to detect the biphasic NSC response, the general viability differences remained unchanged. In agreement with the single culture studies, stem cell viability was higher compared to tumours only at levels around 10 μM.

This study describes the initial proof of principle steps in the technical development of a novel assay. There are a number of future experiments that need to be performed in order to better characterise the model in terms of biology and wider range of responses. A larger number of compounds needs to be screened including neurotoxic anticancer drugs like vincristine, methotrexate and cisplatin as well as drugs without any reported neurotoxicity. The assay would also profit from the addition of wider variety tumour cell lines that recapitulate all four types of medulloblastoma.

Finally, the physiological relevance of this *in vitro* system might be further improved by including an additional differentiation and maturation step in the culture of human neural stem cells. Establishing the proportion of early progenitors, oligodendrocytes, astrocytes and neurons in the model and determining the effects of etoposide and other drugs on each population would further benefit our understanding of cytotoxic mode of action and neurotoxic side effects. Thorough histological characterisation of both the tumour and normal tissue components would also enrich the model. The utilisation of patient-derived primary tumour tissue would allow for a better representation of tumour heterogeneity and holds potential in personalising therapy.

5. Conclusions

This 3D co-culture model includes biorelevant physiological gradients of nutrients and oxygen, natural cell-cell and cell-matrix interactions and the interplay between normal and tumour tissue. It does so without sacrificing throughput and the options for complete automation. The unique combination of a universal cell marking procedure along with flow cytometry and multiphoton imaging make it possible to visualise the interaction between tumour and host tissue and to quantify the effects of cytotoxic drugs on both populations. This proof of concept study suggests a robust method for co-culture creation and analysis that can be used in a universal way to study interaction between any two types of tissue and drugs of interest.

Acknowledgements

We would like to thank Adrian Robins, Nina Lane, David Onion and Nicola Croxall from the Flow cytometry facility at the University of Nottingham for their guidance and assistance with designing and carrying out the experiments. The authors are also grateful to Tim Self for his help in making the multiphoton microscopy studies possible. This study was funded by the joint EPSRC and AstraZeneca Centre for Doctoral Training in Targeted therapeutics-EP/D501849/1.

References

Amann, A., Zwierzina, M., Gamerith, G., Bitsche, M., Huber, J.M., Vogel, G.F., Blumer, M., Koeck, S., Pechriggl, E.J., Kelm, J.M., Hilbe, W., Zwierzina, H., 2014. Development of an innovative 3D cell culture system to study tumour–stroma interactions in non-small cell lung cancer cells. PLoS One 9, e92511, http://dx.doi.org/10.1371/journal.pone.0092511.

Astashkina, A., Mann, B., Grainger, D.W., 2012. A critical evaluation of in vitro cell culture models for high-throughput drug screening and toxicity. Pharmacol. Ther. 134, 82–106, http://dx.doi.org/10.1016/j.pharmthera.2012.01.001.

Attenello, F., Mukherjee, D., Datoo, G., McGirt, M., Bohan, E., Weingart, J., Olivi, A., Quinones-Hinojosa, A., Brem, H., 2008. Use of gliadel (BCNU) wafer in the surgical treatment of malignant glioma: A 10-Year institutional experience. Ann. Surg. Oncol. 15, 2887–2893.

Barbaro, N.M., Gupta, N., Kunwar, S., 2004. Unique astrocyte ribbon in adult human brain contains neural stem cells but lacks chain migration 427, 740–744, http://dx.doi.org/10.1038/nature02298.1.

Barua, N.U., Lowis, S.P., Woolley, M., O'Sullivan, S., Harrison, R., Gill, S.S., 2013. Robot-guided convection-enhanced delivery of carboplatin for advanced brainstem glioma. Acta Neurochir. (Wien). 155, 1459–1465, http://dx.doi.org/10.1007/s00701-013-1700-6.

Begum, J., Day, W., Henderson, C., Purewal, S., Cerveira, J., Summers, H., Rees, P., Davies, D., Filby, A., 2013. A method for evaluating the use of fluorescent dyes to track proliferation in cell lines by dye dilution. Cytometry. A 83, 1085–1095, http://dx.doi.org/10.1002/cyto.a.22403.

Bhojwani, D., Sabin, N.D., Pei, D., Yang, J.J., Khan, R.B., Panetta, J.C., Krull, K.R., Inaba, H., Rubnitz, J.E., Metzger, M.L., Howard, S.C., Ribeiro, R.C., Cheng, C., Reddick, W.E., Jeha, S., Sandlund, J.T., Evans, W.E., Pui, C.-H., Relling, M.V., 2014. Methotrexate-induced neurotoxicity and leukoencephalopathy in childhood acute lymphoblastic leukemia. J. Clin. Oncol. 32, 949–959, http://dx.doi.org/10.1200/JCO.;1; 2013.53.0808.

Carpenter, M.K., Cui, X., Hu, Z., Jackson, J., Sherman, S., Wahlberg, L.U., 1999. In vitro expansion of a multipotent population of human neural progenitor cells 278, 265–278.

Carrera, S., de Verdier, P.J., Khan, Z., Zhao, B., Mahale, A., Bowman, K.J., Zainol, M., Jones, G.D.D., Lee, S.W., Aaronson, S.A., Macip, S., 2010. Protection of cells in physiological oxygen tensions against DNA damage-induced apoptosis. J. Biol. Chem. 285, 13658–13665, http://dx.doi.org/10.1074/jbc.M109.062562.

Chambers, K.F., Pearson, J.F., Aziz, N., O'Toole, P., Garrod, D., Lang, S.H., 2011. Stroma regulates increased epithelial lateral cell adhesion in 3D culture: a role for actin/cadherin dynamics. PLoS One 6, e18796, http://dx.doi.org/10.1371/journal.pone.0018796.

Chintala, S.K., Fueyo, J., Gomez-Manzano, C., Venkaiah, B., Bjerkvig, R., Yung, W.K., Sawaya, R., Kyritsis, a.P., Rao, J.S., 1997. Adenovirus-mediated p16/CDKN2 gene transfer suppresses glioma invasion in vitro. Oncogene 15, 2049–2057, http://dx.doi.org/10.1038/sj.onc.1201382.

Conroy, S., Garnett, M., Vloeberghs, M., Grundy, R., Craven, I., Walker, D., 2010. Medulloblastoma in childhood: revisiting intrathecal therapy in infants and children. Cancer Chemother. Pharmacol. 65, 1173–1189.

Cukierman, E., Pankov, R., Stevens, D.R., Yamada, K.M., 2001. Taking cell-matrix adhesions to the third dimension. Science 294, 1708–1712, http://dx.doi.org/10.1126/science.1064829.

Deeken, J.F., Löscher, W., 2007. The blood-brain barrier and cancer: transporters, treatment, and Trojan horses. Clin. Cancer Res. 13, 1663–1674, http://dx.doi.org/10.1158/1078-0432.CCR-06-2854.

Dietrich, J., Han, R., Yang, Y., Mayer-Pröschel, M., Noble, M., 2006. CNS progenitor cells and oligodendrocytes are targets of chemotherapeutic agents in vitro and in vivo. J. Biol. 5, 22, http://dx.doi.org/10.1186/jbiol50.

Duggan, R., 2012. Ryan Duggan's three step approach to gating Annexin V data appropriately [WWW Document]. URL http://ucflow.blogspot.co.uk/2012/07/my-3-step-approach-to-gating-annexin-v.html

Fang, C., Avis, I., Salomon, D., Cuttitta, F., 2013. Novel phenotypic fluorescent three-dimensional platforms for high-throughput drug screening and personalized chemotherapy. J. Cancer 4, 402–415, http://dx.doi.org/10.7150/jca.6780.

Fleischhack, G., Reif, S., Hasan, C., Jaehde, U., Hettmer, S., Bode, U., 2001. Feasibility of intraventricular administration of etoposide in patients with metastatic brain tumours. Br. J. Cancer 84, 1453–1459.

Foty, R.A., Steinberg, M.S., 2005. The differential adhesion hypothesis: a direct evaluation. Dev. Biol. 278, 255–263, http://dx.doi.org/10.1016/j.ydbio.2004.11.012.

Gállego Pérez-Larraya, J., Palma, J.A., Carmona-Iragui, M., Fernández-Torrón, R., Irimia, P., Rodríguez-Otero, P., Panizo, C., Martínez-Vila, E., 2011. Neurologic complications of intrathecal liposomal cytarabine administered prophylactically to patients with non-Hodgkin lymphoma. J. Neurooncol. 103, 603–609, http://dx.doi.org/10.1007/s11060-010-0428-x.

Go, Y., Chintala, S.K., Mohanam, S., Gokaslan, Z., Venkaiah, B., Bjerkvig, R., Oka, K., Nicolson, G.L., Sawaya, R., Rao, J.S., 1997. Inhibition of in vivo tumorigenicity and invasiveness of a human glioblastoma cell line transfected with antisense uPAR vectors. Clin. Exp. Metastasis 15, 440–446.

Gregg, R.W., Molepo, J.M., Monpetit, V.J., Mikael, N.Z., Redmond, D., Gadia, M., Stewart, D.J., 1992. Cisplatin neurotoxicity: the relationship between dosage, time, and platinum concentration in neurologic tissues, and morphologic evidence of toxicity. J. Clin. Oncol. 10, 795–803.

Hay, M., Thomas, D.W., Craighead, J.L., Economides, C., Rosenthal, J., 2014. Clinical development success rates for investigational drugs. Nat. Biotechnol. 32, 40–51, http://dx.doi.org/10.1038/nbt.2786.

Hickman, J.a., Graeser, R., de Hoogt, R., Vidic, S., Brito, C., Gutekunst, M., van der Kuip, H., 2014. Three-dimensional models of cancer for pharmacology and cancer cell biology: capturing tumor complexity in vitro/ex vivo. Biotechnol. J. 9, 1115–1128, http://dx.doi.org/10.1002/biot.201300492.

Honig, M.G., Hume, R.I., 1986. Fluorescent carbocyanine dyes allow living neurons of identified origin to be studied in long-term cultures. J. Cell Biol. 103, 171–187.

Hsiao, A.Y., Torisawa, Y., Tung, Y.-C., Sud, S., Taichman, R.S., Pienta, K.J., Takayama, S., 2009. Microfluidic system for formation of PC-3 prostate cancer co-culture spheroids. Biomaterials 30, 3020–3027, http://dx.doi.org/10.1016/j.biomaterials.2009.02.047.

Indovina, P., Collini, M., Chirico, G., Santini, M.T., 2007. Three-dimensional cell organization leads to almost immediate HRE activity as demonstrated by molecular imaging of MG-63 spheroids using two-photon excitation microscopy. FEBS Lett. 581, 719–726, http://dx.doi.org/10.1016/j.febslet.2007.01.040.

Ivanov, D.P., Parker, T.L., Walker, D.A., Alexander, C., Ashford, M.B., Gellert, P.R., Garnett, M.C., 2014. Multiplexing spheroid volume, resazurin and acid phosphatase viability assays for high-throughput screening of tumour spheroids and stem cell neurospheres. PLoS One 9, e103817, http://dx.doi.org/10.1371/journal.pone.0103817.

Keles, G.E., Berger, M.S., Srinivasan, J., Kolstoe, D.D., Bobola, M.S., Silber, J.R., 1995. Establishment and characterization of four human medulloblastoma-derived cell lines. Oncol. Res. 7, 493–503.

Khoshyomn, S., Penar, P.L., McBride, W.J., Taatjes, D.J., 1998. Four-dimensional analysis of human brain tumor spheroid invasion into fetal rat brain aggregates using confocal scanning laser microscopy. J. Neurooncol. 38, 1–10.

Kilani, R.T., Tamimi, Y., Hanel, E.G., Wong, K.K., Karmali, S., Lee, P.W.K., Moore, R.B., 2003. Selective reovirus killing of bladder cancer in a co-culture spheroid model. Virus Res. 93, 1–12, http://dx.doi.org/10.1016/S0168-1702(03)00045-5.

Kilani, R.T., Tamimi, Y., Karmali, S., Mackey, J., Hanel, E.G., Wong, K.K., Moore, R.B., 2002. Selective cytotoxicity of gemcitabine in bladder cancer cell lines. Anticancer. Drugs 13, 557–566.

König, K., Uchugonova, A., Gorjup, E., 2011. Multiphoton fluorescence lifetime imaging of 3D-stem cell spheroids during differentiation. Microsc. Res. Tech. 74, 9–17, http://dx.doi.org/10.1002/jemt.20866.

Kool, M., Jones, D.T.W., Jäger, N., Northcott, P., a, Pugh, T.J., Hovestadt, V., Piro, R.M., Esparza, L.A., Markant, S.L., Remke, M., Milde, T., Bourdeaut, F., Ryzhova, M., Sturm, D., Pfaff, E., Stark, S., Hutter, S., Seker-Cin, H., Johann, P., Bender, S., Schmidt, C., Rausch, T., Shih, D., Reimand, J., Sieber, L., Wittmann, A., Linke, L., Witt, H., Weber, U.D., Zapatka, M., König, R., Beroukhim, R., Bergthold, G., van Sluis, P., Volckmann, R., Koster, J., Versteeg, R., Schmidt, S., Wolf, S., Lawerenz, C., Bartholomae, C.C., von Kalle, C., Unterberg, A., Herold-Mende, C., Hofer, S., Kulozik, A.E., von Deimling, A., Scheurlen, W., Felsberg, J., Reifenberger, G., Hasselblatt, M., Crawford, J.R., Grant, G.a., Jabado, N., Perry, A., Cowdrey, C., Croul, S., Zadeh, G., Korbel, J.O., Doz, F., Delattre, O., Bader, G.D., McCabe, M.G., Collins, V.P., Kieran, M.W., Cho, Y.-J., Pomeroy, S.L., Witt, O., Brors, B., Taylor, M.D., Schüller, U., Korshunov, A., Eils, R., Wechsler-Reya, R.J., Lichter, P., Pfister, S.M., 2014. Genome sequencing of SHH medulloblastoma predicts genotype-related response to smoothened inhibition. Cancer Cell 25, 393–405, http://dx.doi.org/10.1016/j.ccr.2014.02.004.

Koopman, G., Reutelingsperger, C.P., Kuijten, G.a., Keehnen, R.M., Pals, S.T., van Oers, M.H., 1994. Annexin V for flow cytometric detection of phosphatidylserine expression on B cells undergoing apoptosis. Blood 84, 1415–1420.

L Berg, E., Hsu, Y.-C., Lee, J.A., 2014. Consideration of the cellular microenvironment: physiologically relevant co-culture systems in drug discovery. Adv. Drug Deliv. Rev. 69–70, 190–204, http://dx.doi.org/10.1016/j.addr.2014.01.013.

Langley, R.R., Fidler, I.J., 2011. The seed and soil hypothesis revisited–the role of tumor-stroma interactions in metastasis to different organs. Int. J. Cancer 128, 2527–2535, http://dx.doi.org/10.1002/ijc.26031.

Lassailly, F., Griessinger, E., Bonnet, D., 2010. Microenvironmental contaminations induced by fluorescent lipophilic dyes used for noninvasive in vitro and in vivo cell tracking. Blood 115, 5347–5354, http://dx.doi.org/10.1182/blood-2009-05-224030.

Luo, C., Johnston, P.J., MacPhail, S.H., Banáth, J.P., Oloumi, A., Olive, P.L., 1998. Cell fusion studies to examine the mechanism for etoposide resistance in Chinese hamster V79 spheroids. Exp. Cell Res. 243, 282–289, http://dx.doi.org/10.1006/excr.1998.4170.

Meng, W., 2006. Evaluation of a nanoparticle drug delivery vehicle in medulloblastoma and organotypic brain cell cultures. University of Nottingham.

Meng, W., Kallinteri, P., Walker, D.A., Parker, T.L., Garnett, M.C., 2007. Evaluation of poly (glycerol-adipate) nanoparticle uptake in an in vitro 3-D brain tumor co-culture model. Exp. Biol. Med. (Maywood). 232, 1100–1108, http://dx.doi.org/10.3181/0612-RM-301.

Muldoon, L.L., Soussain, C., Jahnke, K., Johanson, C., Siegal, T., Smith, Q.R., Hall, W.a., Hynynen, K., Senter, P.D., Peereboom, D.M., Neuwelt, E.a., 2007. Chemotherapy delivery issues in central nervous system malignancy: a reality check. J. Clin. Oncol. 25, 2295–2305, http://dx.doi.org/10.1200/JCO.2006.09.9861.

Nagato, M., Heike, T., Kato, T., Yamanaka, Y., Yoshimoto, M., Shimazaki, T., Okano, H., Nakahata, T., 2005. Prospective characterization of neural stem cells by flow cytometry analysis using a combination of surface markers. J. Neurosci. Res. 80, 456–466, http://dx.doi.org/10.1002/jnr.20442.

Nam, C., Doi, K., Nakayama, H., 2010. Etoposide induces G2/M arrest and apoptosis in neural progenitor cells via DNA damage and an ATM/p53-related pathway. Histol. Histopathol. 25, 485–493.

Nör, C., Sassi, F.A., de Farias, C.B., Schwartsmann, G., Abujamra, A.L., Lenz, G., Brunetto, A.L., Roesler, R., 2013. The histone deacetylase inhibitor sodium butyrate promotes cell death and differentiation and reduces neurosphere formation in human medulloblastoma cells. Mol. Neurobiol. 48, 533–543, http://dx.doi.org/10.1007/s12035-013-8441-7.

Nygaard, S.J., Haugland, H.K., Laerum, O.D., Lund-Johansen, M., Bjerkvig, R., Tysnes, O.B., 1998. Dynamic determination of human glioma invasion in vitro. J. Neurosurg. 89, 441–447, http://dx.doi.org/10.3171/jns.1998.89.3.0441.

Nygaard, S.J., Pedersen, P.H., Mikkelsen, T., Terzis, A.J., Tysnes, O.B., Bjerkvig, R., 1995. Glioma cell invasion visualized by scanning confocal laser microscopy in an in vitro co-culture system. Invasion Metastasis 15, 179–188.

Othman, R.T., Kimishi, I., Bradshaw, T.D., Storer, L.C.D., Korshunov, A., Pfister, S.M., Grundy, R.G., Kerr, I.D., Coyle, B., 2014. Overcoming multiple drug resistance mechanisms in medulloblastoma. Acta Neuropathol. Commun. 2, 57, http://dx.doi.org/10.1186/2051-5960-2-57.

Pambid, M.R., Berns, R., Adomat, H.H., Hu, K., Triscott, J., Maurer, N., Zisman, N., Ramaswamy, V., Hawkins, C.E., Taylor, M.D., Dunham, C., Guns, E., Dunn, S.E., 2014. Overcoming resistance to Sonic Hedgehog inhibition by targeting p90 ribosomal S6 kinase in pediatric medulloblastoma. Pediatr. Blood Cancer 61, 107–115, http://dx.doi.org/10.1002/pbc.24675.

Parish, C.R., 1999. Fluorescent dyes for lymphocyte migration and proliferation studies. Immunol. Cell Biol. 77, 499–508, http://dx.doi.org/10.1046/j.1440-1711.1999.00877.x.

Phan-Lai, V., Florczyk, S.J., Kievit, F.M., Wang, K., Gad, E., Disis, M.L., Zhang, M., 2013. Three-dimensional scaffolds to evaluate tumor associated fibroblast-mediated suppression of breast tumor specific T cells. Biomacromolecules 14, 1330–1337, http://dx.doi.org/10.1021/bm301928u.

Quah, B.J.C., Parish, C.R., 2012. New and improved methods for measuring lymphocyte proliferation in vitro and in vivo using CFSE-like fluorescent dyes. J. Immunol. Methods 379, 1–14, http://dx.doi.org/10.1016/j.jim.2012.02.012.

Quiñones-Hinojosa, A., Chaichana, K., 2007. The human subventricular zone: a source of new cells and a potential source of brain tumors. Exp. Neurol. 205, 313–324, http://dx.doi.org/10.1016/j.expneurol.2007.03.016.

Rahman, C.V., Smith, S.J., Morgan, P.S., Langmack, K.A., Clarke, P.A., Ritchie, A.A., Macarthur, D.C., Rose, F.R., Shakesheff, K.M., Grundy, R.G., Ruman Rahman, 2013. Adjuvant chemotherapy for brain tumors delivered via a novel intra-cavity moldable polymer matrix. PLoS One 8, e77435, http://dx.doi.org/10.1371/journal.pone.0077435.

Ramaswamy, V., Remke, M., Bouffet, E., Faria, C.C., Perreault, S., Cho, Y.-J., Shih, D.J., Luu, B., Dubuc, A.M., Northcott, P.a., Schüller, U., Gururangan, S., McLendon, R., Bigner, D., Fouladi, M., Ligon, K.L., Pomeroy, S.L., Dunn, S., Triscott, J., Jabado, N., Fontebasso, A., Jones, D.T.W., Kool, M., Karajannis, M.a.,

Gardner, S.L., Zagzag, D., Nunes, S., Pimentel, J., Mora, J., Lipp, E., Walter, A.W., Ryzhova, M., Zheludkova, O., Kumirova, E., Alshami, J., Croul, S.E., Rutka, J.T., Hawkins, C., Tabori, U., Codispoti, K.-E.T., Packer, R.J., Pfister, S.M., Korshunov, A., Taylor, M.D., 2013. Recurrence patterns across medulloblastoma subgroups: an integrated clinical and molecular analysis. Lancet Oncol. 14, 1200–1207, http://dx.doi.org/10.1016/S1470-2045(13)70449-2.

Rangarajan, A., Hong, S.J., Gifford, A., Weinberg, R.A., 2004. Species- and cell type-specific requirements for cellular transformation. Cancer Cell 6, 171–183, http://dx.doi.org/10.1016/j.ccr.2004.07.009.

Samlowski, W.E., Robertson, B.A., Draper, B.K., Prystas, E., McGregor, J.R., 1991. Effects of supravital fluorochromes used to analyze the in vivo homing of murine lymphocytes on cellular function. J. Immunol. Methods 144, 101–115, http://dx.doi.org/10.1016/0022-1759(91)90236-9.

Shen, D.D., Artru, A.a., Adkison, K.K., 2004. Principles and applicability of CSF sampling for the assessment of CNS drug delivery and pharmacodynamics. Adv. Drug Deliv. Rev. 56, 1825–1857, http://dx.doi.org/10.1016/j.addr.2004.07.011.

Shih, D.J.H., Northcott, P.a., Remke, M., Korshunov, A., Ramaswamy, V., Kool, M., Luu, B., Yao, Y., Wang, X., Dubuc, A.M., Garzia, L., Peacock, J., Mack, S.C., Wu, X., Rolider, A., Morrissy, a.S., Cavalli, F.M.G., Jones, D.T.W., Zitterbart, K., Faria, C.C., Schüller, U., Kren, L., Kumabe, T., Tominaga, T., Shin Ra, Y., Garami, M., Hauser, P., Chan, J.a., Robinson, S., Bognár, L., Klekner, A., Saad, A.G., Liau, L.M., Albrecht, S., Fontebasso, A., Cinalli, G., De Antonellis, P., Zollo, M., Cooper, M.K., Thompson, R.C., Bailey, S., Lindsey, J.C., Di Rocco, C., Massimi, L., Michiels, E.M.C., Scherer, S.W., Phillips, J.J., Gupta, N., Fan, X., Muraszko, K.M., Vibhakar, R., Eberhart, C.G., Fouladi, M., Lach, B., Jung, S., Wechsler-Reya, R.J., Fèvre-Montange, M., Jouvet, A., Jabado, N., Pollack, I.F., Weiss, W.a., Lee, J.-Y., Cho, B.-K., Kim, S.-K., Wang, K.-C., Leonard, J.R., Rubin, J.B., de Torres, C., Lavarino, C., Mora, J., Cho, Y.-J., Tabori, U., Olson, J.M., Gajjar, A., Packer, R.J., Rutkowski, S., Pomeroy, S.L., French, P.J., Kloosterhof, N.K., Kros, J.M., Van Meir, E.G., Clifford, S.C., Bourdeaut, F., Delattre, O., Doz, F.F., Hawkins, C.E., Malkin, D., Grajkowska, W.a., Perek-Polnik, M., Bouffet, E., Rutka, J.T., Pfister, S.M., Taylor, M.D., 2014. Cytogenetic prognostication within medulloblastoma subgroups. J. Clin. Oncol. 32, 886–896, http://dx.doi.org/10.1200/JCO.2013.50.9539.

Shuper, a., Stark, B., Kornreich, L., Cohen, I.J., Aviner, S., Steinmetz, a., Stein, J., Goshen, Y., Yaniv, I., 2000. Methotrexate treatment protocols and the central nervous system: significant cure with significant neurotoxicity. J. Child Neurol. 15, 573–580, http://dx.doi.org/10.1177/088307380001500902.

Slavc, I., Schuller, E., Falger, J., Günes, M., Pillwein, K., Czech, T., Dietrich, W., Rössler, K., Dieckmann, K., Prayer, D., Hainfellner, J., 2003. Feasibility of long-term intraventricular therapy with mafosfamide (n = 26) and etoposide (n = 11): experience in 26 children with disseminated malignant brain tumors. J. Neurooncol. 64, 239–247.

Spink, B.C., Cole, R.W., Katz, B.H., Gierthy, J.F., Bradley, L.M., Spink, D.C., 2006. Inhibition of MCF-7 breast cancer cell proliferation by MCF-10A breast epithelial cells in coculture. Cell Biol. Int. 30, 227–238, http://dx.doi.org/10.1016/j.cellbi.2005.11.006.

Srivastava, V.K., Nalbantoglu, J., 2008. Flow cytometric characterization of the DAOY medulloblastoma cell line for the cancer stem-like phenotype. Cytometry. A 73, 940–948, http://dx.doi.org/10.1002/cyto.a.20633.

Straussman, R., Morikawa, T., Shee, K., Barzily-Rokni, M., Qian, Z.R., Du, J., Davis, A., Mongare, M.M., Gould, J., Frederick, D.T., Cooper, Z.A., Chapman, P.B., Solit, D.B., Ribas, A., Lo, R.S., Flaherty, K.T., Ogino, S., Wargo, J.A., Golub, T.R., 2012. Tumour micro-environment elicits innate resistance to RAF inhibitors through HGF secretion. Nature 487, 500–504, http://dx.doi.org/10.1038/nature11183.

Taylor, M.D., Northcott, P.a., Korshunov, A., Remke, M., Cho, Y.-J., Clifford, S.C., Eberhart, C.G., Parsons, D.W., Rutkowski, S., Gajjar, A., Ellison, D.W., Lichter, P., Gilbertson, R.J., Pomeroy, S.L., Kool, M., Pfister, S.M., 2012. Molecular subgroups of medulloblastoma: the current consensus. Acta Neuropathol. 123, 465–472, http://dx.doi.org/10.1007/s00401-011-0922-z.

Terzis, A.J., Dietze, A., Vig, R.B., Old, H.A.R.N., 1997a. Effects of photodynam ic therapy on gliom a spheroids 11, 196–205.

Terzis, A.J., Thorsen, F., Heese, O., Visted, T., Bjerkvig, R., Dahl, O., Arnold, H., Gundersen, G., 1997b. Proliferation, migration and invasion of human glioma cells exposed to paclitaxel (Taxol) in vitro. Br. J. Cancer 75, 1744–1752.

Thorsen, F., Visted, T., Lehtolainen, P., Ylä-Herttuala, S., Bjerkvig, R., 1997. Release of replication-deficient retroviruses from a packaging cell line: interaction with glioma tumor spheroids in vitro. Int. J. Cancer 71, 874–880.

Tomlinson, F.H., Lihou, M.G., Smith, P.J., 1991. Comparison of in vitro activity of epipodophyllotoxins with other chemotherapeutic agents in human medulloblastomas. Br. J. Cancer 64, 1051–1059.

Uchida, N., Buck, D.W., He, D., Reitsma, M.J., Masek, M., Phan, T.V., Tsukamoto, A.S., Gage, F.H., Weissman, I.L., 2000. Direct isolation of human central nervous system stem cells. Proc. Natl. Acad. Sci. 97, 14720–14725, http://dx.doi.org/10.1073/pnas.97.26.14720.

Upreti, M., Jamshidi-Parsian, A., Koonce, N.A., Webber, J.S., Sharma, S.K., Asea, A.A., Mader, M.J., Griffin, R.J., 2011. Tumor-endothelial cell three-dimensional spheroids: new aspects to enhance radiation and drug therapeutics. Transl. Oncol. 4, 365–376.

Urich, E., Patsch, C., Aigner, S., Graf, M., Iacone, R., Freskgård, P.-O., 2013. Multicellular self-assembled spheroidal model of the blood brain barrier. Sci. Rep. 3, 1500, http://dx.doi.org/10.1038/srep01500.

Van der Gaast, A., Sonneveld, P., Mans, D.R., Splinter, T.A., 1992. Intrathecal administration of etoposide in the treatment of malignant meningitis: feasibility and pharmacokinetic data. Cancer Chemother. Pharmacol. 29, 335–337.

Vanner, R.J., Remke, M., Gallo, M., Selvadurai, H.J., Coutinho, F., Lee, L., Kushida, M., Head, R., Morrissy, S., Zhu, X., Aviv, T., Voisin, V., Clarke, I.D., Li, Y., Mungall, A.J., Moore, R.a., Ma, Y., Jones, S.J.M., Marra, M.a., Malkin, D., Northcott, P.a., Kool, M., Pfister, S.M., Bader, G., Hochedlinger, K., Korshunov, A., Taylor, M.D., Dirks, P.B., 2014. Quiescent Sox2(+) cells drive hierarchical growth and relapse in sonic hedgehog subgroup medulloblastoma. Cancer Cell 1–15, http://dx.doi.org/10.1016/j.ccr.2014.05.005.

Von Bueren, A.O., Oehler, C., Shalaby, T., von Hoff, K., Pruschy, M., Seifert, B., Gerber, N.U., Warmuth-Metz, M., Stearns, D., Eberhart, C.G., Kortmann, R.D., Rutkowski, S., Grotzer, M.a., 2011. c-MYC expression sensitizes medulloblastoma cells to radio- and chemotherapy and has no impact on response in medulloblastoma patients. BMC Cancer 11, 74, http://dx.doi.org/10.1186/1471-2407-11-74.

Wartenberg, M., 2001. Tumor-induced angiogenesis studied in confrontation cultures of multicellular tumor spheroids and embryoid bodies grown from pluripotent embryonic stem cells. FASEB J. 15, 995–1005, http://dx.doi.org/10.1096/fj.00-0350com.

Weston, S.A., Parish, C.R., 1990. New fluorescent dyes for lymphocyte migration studies, analysis by flow cytometry and fluorescence microscopy. J. Immunol. Methods 133, 87–97.

Zanini, C., Ercole, E., Mandili, G., Salaroli, R., Poli, A., Renna, C., Papa, V., Cenacchi, G., Forni, M., 2013. Medullospheres from DAOY, UW228 and ONS-76 cells: increased stem cell population and proteomic modifications. PLoS One 8, e63748, http://dx.doi.org/10.1371/journal.pone.0063748.

Zembruski, N.C.L., Stache, V., Haefeli, W.E., Weiss, J., 2012. 7-Aminoactinomycin D for apoptosis staining in flow cytometry. Anal. Biochem. 429, 79–81, http://dx.doi.org/10.1016/j.ab.2012.07.005.